PHYSICAL REVIEW D **95,** 095005 (2017)

Scalar unparticle signals at the LHC

T. M. Aliev,[1,*] S. Bilmiş,[1,†] M. Solmaz,[2,‡] and I. Turan[1,§]

[1]*Department of Physics, Middle East Technical University, Ankara 06800, Turkey*

[2]*Physics Department, University of California, Santa Barbara, California 93106-9530, USA*

(Received 6 January 2017; published 8 May 2017)

If scale invariance exists in nature, the so-called "unparticle physics" may become part of reality. The only way to refute or confirm this idea is through experiments, such as those at the Large Hadron Collider (LHC). One of the peculiar properties of the unparticle stuff is that it gives striking multiphoton signals which have been studied through only the unparticle self-interactions. By considering not only the self-interactions of unparticles but also all the other possible contributions, which are dominant, a detailed study of the processes, within a scalar unparticle scenario, $pp \to 4\gamma$, $pp \to 2\gamma 2g$, $pp \to 2\gamma 2\ell$, $pp \to 4e$, $pp \to 4\mu$ and $pp \to 2e2\mu$ at $\sqrt{s} = 14$ TeV at the LHC is carried out. We use basic selection cuts and analyze various distributions to discriminate the signals over the Standard Model backgrounds and discuss what seems to be the most likely channel among the above for an indirect manifestation of unparticle effects. We follow a new approach to tackle the issue with the three-point correlation function for the scalar unparticle self-interactions. We also obtain the exclusion region in the unparticle parameter space from the available two-photon data of the LHC and compare it with the existing bounds coming from other sources.

DOI: 10.1103/PhysRevD.95.095005

I. INTRODUCTION

Since the discovery of the Higgs particle at the Large Hadron Collider (LHC) at CERN [1,2], the particle content of the Standard Model (SM) has finally been completed after many years of desperate searching. Despite the fact that the SM is extremely successful at describing all the existing experimental data, it had still been lacking mechanisms to explain some unsolved problems. For example, the SM could not address the issue about mechanism for neutrino masses, can not incorporate gravitational interactions, has no dark matter candidate, subsumes the so-called hierarchy problem, etc. Having the Higgs particle at hand, the following three distinct directions will shape the search programs in the current and upcoming experiments:

(i) Making precise measurements of the Higgs decay channels, the Yukawa couplings, etc.
(ii) Improving the precision to measure the properties of the SM particles as well as the electroweak precision parameters such as the electroweak mixing angle, W boson mass, asymmetries, etc.
(iii) Searching for new physics beyond the SM, among the vast list of which are low-scale supersymmetry, extra dimensions, and the so-called unparticle physics which originates from an entirely different standpoint.

About a decade ago, unparticle physics as a beyond-SM scenario had been introduced in [3,4] based on the low-energy manifestation of a nontrivial scale-invariant effective field theory. In this content, as the simplest choice, a new scalar field (called the scalar unparticle $\mathcal{U}$), which is a singlet under the $SU(2)_L$ group, can couple to photons and gluons directly through higher-dimensional operators with a cutoff scale $\Lambda_{\mathcal{U}}$ below which interpolating fields emerge with some nonintegral scaling dimension $d_{\mathcal{U}}$. The scenario involves rich phenomenology and predicts the existence of scalar unparticle self-interactions [5–8], which could give unusually large effects in gluon fusion processes. For example, the $gg \to \mathcal{U} \to \gamma\gamma$ process leads to enhancement of signals in the Higgs decay channels, and the self-interactions of unparticles give rise to signals with different four-particle states, such as four photons, two photons + two gluons, two photons + two leptons, and four charged leptons. It is interesting that the four-photon signal is practically background free and therefore can play a critical role in the discovery of unparticles (for more details see [7,9]). It has also been shown that in addition to the contribution to some of these processes through the scalar unparticle self-interactions, there are other single and double unparticle exchange diagrams, making significant contributions (even dominating) to these signals [9]. Hence it is essential to do a complete study of such signals including all contributions. Here, we should note and stress the point that in this study we concentrate only on the virtual unparticle contributions to various processes. Obviously one could alternatively search for unparticle effects through their real emissions. We will discuss this point later.

In the present work, we extend the calculations presented in [9] for the processes $pp \to 4\gamma$, $pp \to 2\gamma 2g$ to the LHC energy $\sqrt{s} = 14$ TeV by making a simulation including basic detector effects, as well as analyzing the other

*taliev@metu.edu.tr
†sbilmis@metu.edu.tr
‡msolmaz@hep.ucsb.edu
§ituran@metu.edu.tr

processes with the final states $2\gamma 2\ell$, $e^+e^-e^+e^-$, $\mu^+\mu^-\mu^+\mu^-$, and $e^+e^-\mu^+\mu^-$ at the LHC.

The work is organized as follows. In section II we briefly describe the elements of the unparticle theory, present the specific couplings necessary for our calculations. Unparticle self-interactions and how we treat the vertex function are given in section II A. Section II B covers some details of the scalar unparticle model implementation to MadGraph5. Section III is devoted to the numerical analysis of the processes with four-particle configurations in the final states. In Section IV, we give a summary of our work.

II. THEORETICAL FRAMEWORK

The basic idea of the unparticle theory is the existence of the scale-invariant hidden sector at high energy $\Lambda_{\mathcal{U}}$ and above. Below the $\Lambda_{\mathcal{U}}$ scale, unparticle physics manifests as an interpolating field $\mathcal{O}$ having various scaling dimensions and Lorentz structure. One of the characteristic properties of the unparticle operator is that it has a continuous spectral density,

$$\rho_{\mathcal{U}}(p^2) = A_{d_{\mathcal{U}}}\Theta(p^0)\Theta(p^2)(p^2)^{d_{\mathcal{U}}-2}, \tag{1}$$

where $d_{\mathcal{U}}$ is the scaling dimension and the factor $A_{d_{\mathcal{U}}}$ is determined as

$$A_{d_{\mathcal{U}}} = \frac{16\pi^{5/2}}{(2\pi)^{3/2}}\frac{\Gamma(d_{\mathcal{U}}+1/2)}{\Gamma(d_{\mathcal{U}}-1)\Gamma(2d_{\mathcal{U}})}. \tag{2}$$

From this expression, it follows that when $d_{\mathcal{U}} \to 1$, Eq. (1) reduces to the massless particle phase space. For this reason, one can suggest that unparticle behaves like a collection of $d_{\mathcal{U}}$ number of massless fields. In the rest of the paper, we restrict ourselves by considering only scalar unparticle. The form of propagator for scalar particle is obtained in [8]

$$\Delta_f = \frac{A_{d_{\mathcal{U}}}}{2\sin(\pi d_{\mathcal{U}})}\frac{ie^{i\phi}}{(|p|^2+i\epsilon)^{2-d_{\mathcal{U}}}} \tag{3}$$

The phase ϕ is defined as $\phi = Arg(-p^2)^{d_{\mathcal{U}}}$. It should be noted that the phase is nonzero in s-channel, while in t and u channels it is equal to zero. For the scalar operator, the unitarity condition leads to $d_{\mathcal{U}} \geq 1$ [10]. Unparticle operators can interact with the SM particles via exchange of heavy particle with mass M. After integrating out the heavy degrees of freedom, a series of effective operators describing the interaction of the SM particles with unparticles at low energy are obtained. The operators describing the interactions for scalar unparticle with the SM particles are;

$$\lambda_0'\frac{1}{\Lambda_{\mathcal{U}}^{d_{\mathcal{U}}-1}}\bar{f}f\mathcal{O},$$
$$\lambda_0''\frac{1}{\Lambda_{\mathcal{U}}^{d_{\mathcal{U}}-1}}\bar{f}i\gamma_5 f\mathcal{O},$$
$$\lambda_0\frac{1}{\Lambda_{\mathcal{U}}^{d_{\mathcal{U}}}}G_{\alpha\beta}G^{\alpha\beta}\mathcal{O}. \tag{4}$$

The Feynman rules for the scalar unparticle operators with the gg and $\gamma\gamma$ are

$$4i\lambda_{g,\gamma}^0\frac{1}{\Lambda_{\mathcal{U}}}(-g_{\mu\nu}(p_1\cdot p_2)+p_{1\nu}p_{2\mu}). \tag{5}$$

For the calculation of the signals at hand the following two- and three-point correlation functions need to be evaluated [5,7]

$$\langle 0|\mathcal{O}_{\mathcal{U}}(x)\mathcal{O}_{\mathcal{U}}^{\dagger}(0)|0\rangle = \int\frac{d^4p}{(2\pi)^4}e^{-ipx}\rho_{\mathcal{U}}(p^2), \tag{6}$$

$$\begin{aligned}&\langle 0|\mathcal{O}_{\mathcal{U}}(p_1)\mathcal{O}_{\mathcal{U}}(p_2)\mathcal{O}_{\mathcal{U}}^{\dagger}(p_1+p_2)|0\rangle\\ &= C_d\int\frac{d^4q}{(2\pi)^4}\{[-q^2-i\epsilon][-(p_1-q)^2-i\epsilon]\\ &\quad\times[-(p_2+q)^2-i\epsilon]\}^{d_{\mathcal{U}}/2-2}\\ &= -i(-1)^nC_d\left(\frac{1}{s}\right)^{n-2}F_y\left(\frac{p_1^2}{s},\frac{p_2^2}{s}\right)\end{aligned} \tag{7}$$

where $n = 6(1-d_{\mathcal{U}}/4)$ and $s = (p_1+p_2)^2$. The three-point correlation function is

$$\begin{aligned}F_y\left(\frac{p_1^2}{s},\frac{p_2^2}{s}\right) &= \frac{\Gamma(n-2)}{16\pi^2[\Gamma(\frac{n}{2})]^3}\int_0^1 dx_1dx_2dx_3(x_1x_2x_3)^{\frac{n}{3}-1}\\ &\quad\times\delta(x_1+x_2+x_3-1)\left(\frac{1}{\Delta}\right)^{n-2}\end{aligned} \tag{8}$$

with $\Delta = x_1x_2p_1^2/s + x_1x_3p_2^2/s + x_2x_3$. We take $\lambda_{g,\gamma}^0 = 1$ and $\lambda_0' = \sqrt{2\pi}/e$ which follows from the naturalness requirement. The relevant part of the unparticle model has been implemented in MadGraph5[11] package program in the UFO format. Some of the details of the implementation are summarized below.

A. Unparticle Self-Interaction

The most striking feature of the unparticle scenario is that it enables three-point vertices where a scalar unparticle couples to two other unparticles of the same type and the vertex factor is not of a typical tree level form. Hence it requires special attention. Some promising processes such as $pp \to \gamma\gamma\gamma\gamma$, $pp \to \gamma\gamma gg$, $pp \to \gamma\gamma\ell\ell$, etc. could originate from scalar unparticle self-interactions where the factor C_d in Eq. (7) is indeed free at first. However, see

the discussion in [9] about various phenomenological bounds on C_d and in [12] for theoretical considerations.

In particular, the difficulty behind the computation of the complicated function of F_y in the simulations is related to long hours of CPU time due to the integrals involved in F_y. This has led us to pursue a relatively simpler approach. In this approach, one would not only avoid the time-consuming computation but also make the complete model feasible to implement an event generator programs. For that reason, we decided to make a two-dimensional fitting for the F_y function.

For each value of the scaling dimension parameter, $d_{\mathcal{U}} = \{1.1, 1.2, ..., 1.9\}$, the function F_y has been evaluated via Mathematica with a statistically high number of two-dimensional data grids. Afterward, the tabulated data set for each $d_{\mathcal{U}}$ value has been input in Matlab to get the polynomial functional forms. Several plots are obtained to check if the fitting results are fairly convincing, and some are shown in Fig. 1. The explicit forms of the fitted function F_y are given for various $d_{\mathcal{U}}$ values in Appendix B.

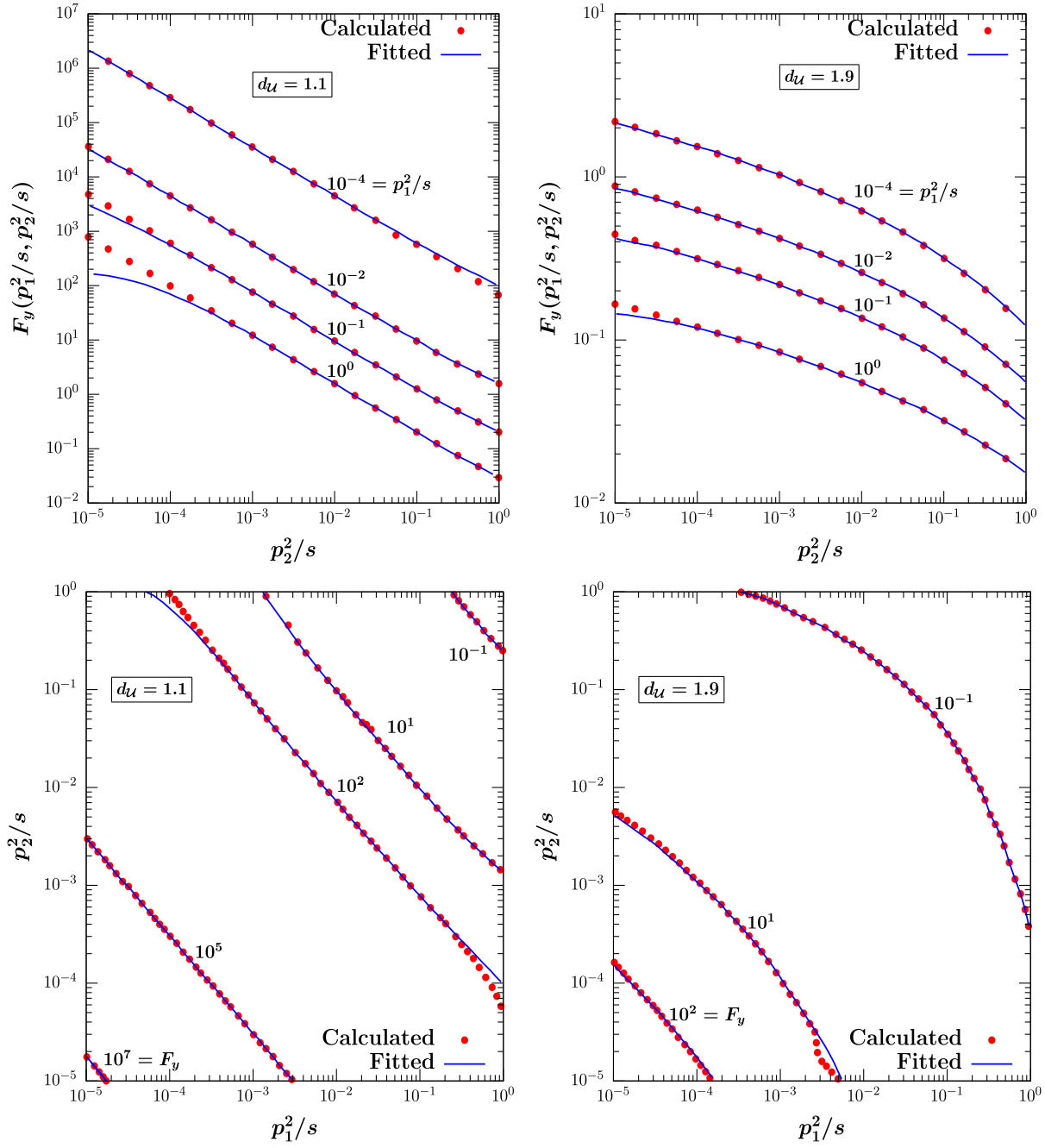

FIG. 1. In the upper row, the three-point correlation function $F_y(p_1^2/s, p_2^2/s)$ is plotted as a function of p_2^2/s for various p_1^2/s values by using both the exact integral form and the polynomial fit functions. In the second row, various values of F_y is depicted in the $(p_1^2/s, p_2^2/s)$.

B. Implementing the unparticle model in MadGraph5

Implementation of the unparticle model in the event generator programs intended for three-level calculations has not been an easy task to achieve due to the structure of the model, such as the nontrivial scalar propagator expression and the three-point correlation function.

An event generator program that would offer vast flexibility in applying nonstraightforward principles would be the best choice, and MadGraph5 fits this purpose. Another reason we chose MadGraph5 is that new physics models can be defined in UFO format [13]. There are a couple of advantages in introducing an unparticle model as a UFO file, one of which is that one may freely write down any Lorentz expression for an arbitrary vertex. In addition, UFO also allows users to define effective vertices with no constraint on the number of particles in each vertex. These features have been employed to define the vertices in the model for further analysis of the signals of the unparticle model.

The unparticles are defined as massless scalars at the Lagrangian level with the FeynRules interface [14]. The additional parameters were also attributed to the model, such as $d_{\mathcal{U}}$ and $\Lambda_{\mathcal{U}}$ and some other coupling constants. In the end, the FeynRules package produces the UFO file of the model containing all the information regarding parameters, couplings, vertices, and Lorentz expressions of each vertex.

Further modifications in the UFO model file are needed to define the unparticle model properly. Then, the processes occurring within the scalar unparticle self-interactions have been introduced to the unparticle model file by setting new effective vertices with two incoming and four outgoing particles, namely, $gg/q\bar{q} \to 4\gamma, 2\gamma 2g, 2\gamma 2\ell, 2e2\mu$. The Feynman diagrams representing these processes are presented in Appendix A. Couplings for these vertices were also added, respectively. Moreover, the stand-alone use of the ALOHA [15] package led us to scrutinize the FORTRAN subroutines that belong to the unparticle model, evaluating the amplitude of each Feynman diagram. In this way, we could embed the unparticle scalar propagator and the three-point correlation function into the corresponding subroutines to get the final model file.

C. Bounds in the $(d_{\mathcal{U}}, \Lambda_{\mathcal{U}})$ plane from $pp \to 2\gamma$ data

Before concentrating on various processes at a center of mass energy of 14 TeV at the LHC, let us check the status of the model in light of the available data. One of the relevant constraints could come from the measurement of an isolated photon pair by the CMS Collaboration at 7 TeV [16] with a data sample corresponding to an integrated luminosity of 36 pb^{-1}, and isolated photons are required to have transverse energies $E_T > 23$ and $E_T > 20$ GeV, respectively.

The experimental analysis is performed in two different pseudorapidity regions—one with $|\eta| < 1.44$ and the other one $|\eta| < 2.5$ but excluding the region $1.44 < |\eta| < 1.57$. The cone size between the photons is assumed $\Delta R > 0.45$. The background events could be like Drell-Yan events with two misidentified electrons as photons, or photon + jet, or multijet events where photons come off hadronic decays. The leading contributions are the $q\bar{q}$ annihilation to a diphoton pair, the diphoton pair through a gluon fusion, and the quark-gluon scattering into a diphoton and jet. The results for the integrated diphoton cross sections are [16]

$$\sigma^{\rm exp}(pp \to \gamma\gamma)|_{|\eta|<1.44} = 31.0 \pm 1.8({\rm stat})^{+2.0}_{-2.1}({\rm syst}) \pm 1.2({\rm lumi})\ {\rm pb},$$

$$\sigma^{\rm exp}(pp \to \gamma\gamma)|_{|\eta|<2.50} = 62.4 \pm 3.6({\rm stat})^{+5.3}_{-5.8}({\rm syst}) \pm 2.5({\rm lumi})\ {\rm pb},$$

while the theoretical calculations within the Standard Model are computed as [16]

$$\sigma^{\rm SM}(pp \to \gamma\gamma)|_{|\eta|<1.44} = 27.3^{+3.0}_{-2.2}({\rm scales}) \pm 1.1\ ({\rm PDF})\ {\rm pb},$$

$$\sigma^{\rm SM}(pp \to \gamma\gamma)|_{|\eta|<2.50} = 52.7^{+5.8}_{-4.2}({\rm scales}) \pm 2.0\ ({\rm PDF})\ {\rm pb}.$$

Here, $|\eta| < 1.44$ and $|\eta| < 2.5$ are the pseudorapidity regions as described above. One can see from these numbers that the measurements are consistent with the SM predictions by taking the experimental and theoretical uncertainties into account.

If one extends the theoretical framework into the unparticle scenario, the theory predictions for the above cross sections would get new indirect contributions as the pure unparticle part, $\sigma^{\rm U}(pp \to \gamma\gamma)$, and the interference, $\sigma^{\rm int}(pp \to \gamma\gamma)$. Using the available room between the experimental and SM values including both the experimental and theoretical errors, one can set limits on the

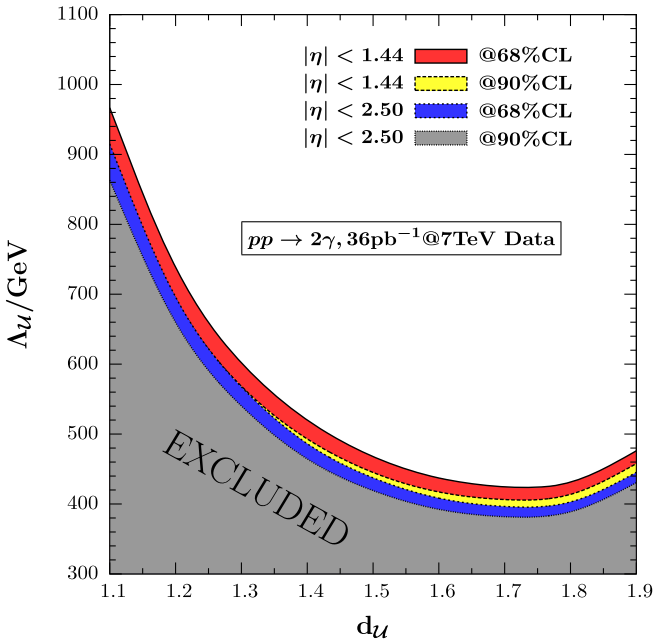

FIG. 2. Using the $pp \to 2\gamma$ data with 36 pb^{-1} at 7 TeV [16], the exclusion plot in the $(d_{\mathcal{U}}, \Lambda_{\mathcal{U}})$ plane is shown at both 68% and 90% C.L.s. Two different pseudorapidity cuts are shown. Both the experimental and the SM errors are included.

parameters of the unparticle model, namely, $d_{\mathcal{U}}$ and $\Lambda_{\mathcal{U}}$. The exclusion limits in the $(d_{\mathcal{U}}, \Lambda_{\mathcal{U}})$ plane are shown in Fig. 2. We present our results for both pseudorapidity regions, $|\eta| < 1.44$ and $|\eta| < 2.5$, at 68% C.L. and 90% C.L. in each case. The bound on $\Lambda_{\mathcal{U}}$ can get as large as 1 TeV for small $d_{\mathcal{U}}$ values, but it is smaller for larger $d_{\mathcal{U}}$ values. Note that the analysis of the SM part in [16] has already been calculated in the next-to-leading order, but we kept the unparticle contribution as well as the interference in the leading order.

It is noted that there are other studies searching unparticle effects by using the LHC data for the reactions monojet + MET (missing transverse energy) and mono-Z + MET [17], putting stringent bounds on $\Lambda_{\mathcal{U}}$. The crucial point in the analyses in [17] is that the unparticles are assumed to be produced as real, and their lifetimes are large enough not to decay inside the detector. Hence, they just create large transverse energy imbalance. On the other hand, in our analysis, the unparticles are all virtual and their effects are seen within the discrepancy between the Monte Carlo simulation and the SM prediction.

III. NUMERICAL ANALYSIS

A numerical analysis will be done by using various kinematical quantities. Let us briefly explain them. If θ and φ represent the polar and azimuthal angles in the barrel, respectively, the distance between the particle i and particle j of an event can be defined as $\Delta R_{ij} = \sqrt{(\Delta\eta_{ij})^2 + (\Delta\varphi_{ij})^2}$, where η_i is the pseudorapidity of the particle i, defined as $\eta_i = -\ln(\tan\frac{\theta_i}{2})$. Here i and j represent any particle in our signals.

Another kinematical quantity is the invariant mass of the ij-particle system and is defined as $m_{ij} = (p_i + p_j)^2$, where $p_i(p_j)$ is the four-momentum of the particle $i(j)$. This definition can be extended to more than two particles as well. Note also that the broad peaks in the invariant mass distributions do not always correspond to the existence of a new particle and care should be given.

There are two more transverse variables to define. One is the usual transverse momentum of, say, particle i, $p_T^i = \sqrt{(p_x^i)^2 + (p_y^i)^2}$ if the beam direction is taken along the z axis. For each event, the objects are listed in the order of decreasing transverse momenta. The other one is the so-called H_T variable, related to p_T^i. H_T is defined as the scalar sum of the p_T^i where i could be jet, lepton, or photon, as well as the missing transverse energy, $\not{E}_T$. That is, $H_T = \not{E}_T + \sum_i |p_T^i|$. Thus, H_T can be taken as a measure of the overall energy scale of the process.

The basic cuts applied for each signal are listed in Table I. All simulations are done by first using MadGraph5 [18] to generate partonic events and then the Pythia [19] event generator is used for hadronization with parton distribution functions CTEQ6L1. The final results are obtained after

TABLE I. The selection cuts imposed for each channel.

$pp \to 4\gamma$	$pp \to 2g2\gamma$	$pp \to 2\gamma 2\ell$	$pp \to 4\ell$
$p_T(\gamma) > 30$ GeV	$p_T(\gamma) > 30$ GeV $p_T(j) > 30$ GeV	$p_T(\gamma) > 30$ GeV $p_T(\ell) > 15$ GeV	$p_T(\ell) > 15$ GeV
$\lvert\eta(\gamma)\rvert < 2.44$	$\lvert\eta(\gamma)\rvert < 2.44$ $\lvert\eta(j)\rvert < 2.44$	$\lvert\eta(\gamma)\rvert < 2.44$ $\lvert\eta(\ell)\rvert < 2.44$	$\lvert\eta(\ell)\rvert < 2.0$
$\Delta R(\gamma,\gamma) > 0.4$	$\Delta R(j,j) > 0.4$ $\Delta R(\gamma,\gamma) > 0.4$ $\Delta R(j,\gamma) > 0.4$	$\Delta R(\ell,\ell) > 0.4$ $\Delta R(\gamma,\gamma) > 0.4$ $\Delta R(\ell,\gamma) > 0.4$	$\Delta R(\ell,\ell) > 0.4$

TABLE II. The total cross sections (in pb) of the signals considered in the study are listed for two cutoff $\Lambda_{\mathcal{U}}$ values, 1 and 3 TeV, and various d values. The cross sections for the Standard Model background are also included for comparison.

Cross-section values (pb)					
	$\Lambda_{\mathcal{U}}$	$d_{\mathcal{U}} = 1.1$	$d_{\mathcal{U}} = 1.5$	$d_{\mathcal{U}} = 1.9$	SM
$pp \to 4\gamma$	1 TeV	9.792×10^{-3}	1.745×10^{-4}	7.665×10^{-4}	8.776×10^{-6}
	3 TeV	1.077×10^{-5}	1.018×10^{-5}	1.017×10^{-5}	
$pp \to 2\gamma 2g$	1 TeV	5.520×10^{1}	3.010×10^{0}	3.798×10^{0}	1.675×10^{-1}
	3 TeV	6.166×10^{-1}	1.826×10^{-1}	1.797×10^{-1}	
$pp \to 2\gamma 2\ell$	1 TeV	8.117×10^{-3}	7.251×10^{-4}	7.716×10^{-4}	4.355×10^{-4}
	3 TeV	5.060×10^{-4}	4.716×10^{-4}	4.713×10^{-4}	
$pp \to 4\ell$	1 TeV	6.310×10^{-4}	4.422×10^{-5}	5.903×10^{-5}	8.586×10^{-6}
	3 TeV	1.304×10^{-5}	1.026×10^{-5}	1.021×10^{-5}	

passing events to PGS to simulate the detector limitations. In Table II, we list the total cross sections for the channels $4\gamma, 2\gamma 2g, 2\gamma 2\ell$, and 4ℓ at $\sqrt{s} = 14$ TeV center-of-mass energy for the following values of $d_{\mathcal{U}}$ and $\Lambda_{\mathcal{U}}$: $(d_{\mathcal{U}}, \Lambda) = (1.1, 1-3\ \text{TeV}), (1.5, 1-3\ \text{TeV}), (1.9, 1-3\ \text{TeV})$. The SM cross sections are also included for background comparison. For almost all signals, the unparticle cross sections are around 2 to 3 orders of magnitude larger than those of the SM for $\Lambda_{\mathcal{U}} = 1$ TeV, but they become almost the same when $\Lambda_{\mathcal{U}} = 3$ TeV. A sizable deviation from the background is possible for $\Lambda_{\mathcal{U}}$ around 1 TeV.

A. $pp \to 4\gamma$ signal

Detecting energetic photons at colliders serves many purposes like testing perturbative QCD [16,20] as well as various commonly used techniques [21]. Their better identification becomes critical since they usually form an important background to various exotic signals of the beyond-SM scenarios [22]. Even though measuring the

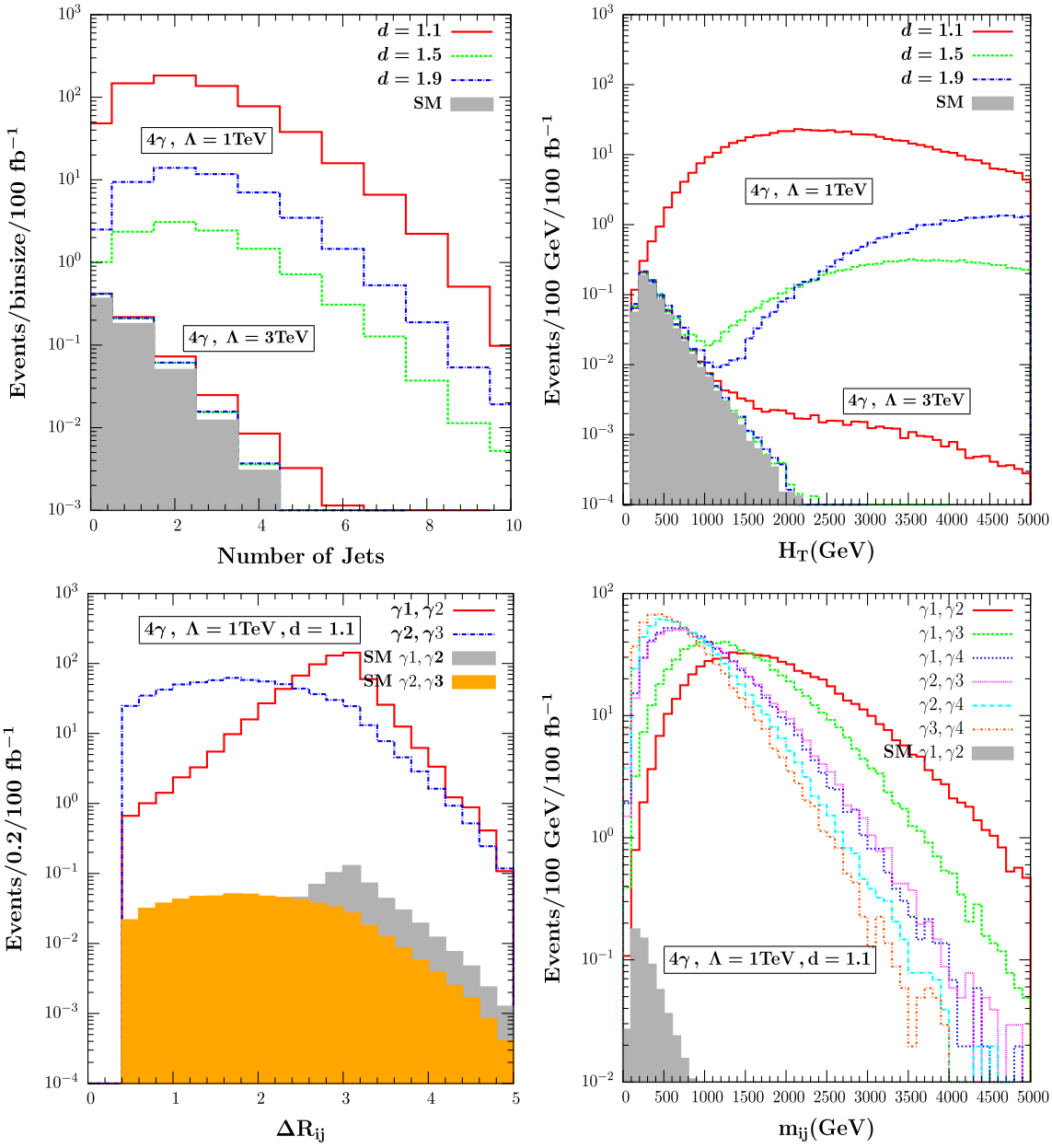

FIG. 3. Various distributions for the $pp \to 4\gamma$ signal at the LHC @ 14 TeV center-of-mass energy within a scalar unparticle scenario for different choices of d and $\Lambda_{\mathcal{U}}$. In the case of the invariant mass distribution, only the largest SM background is shown. For the ΔR_{ij} distributions, two distinct SM backgrounds are preferred to be presented. $\Lambda_{\mathcal{U}} = 3$ TeV case is not included in the ΔR_{ij} and m_{ij} cases since it looks very much like the SM distribution.

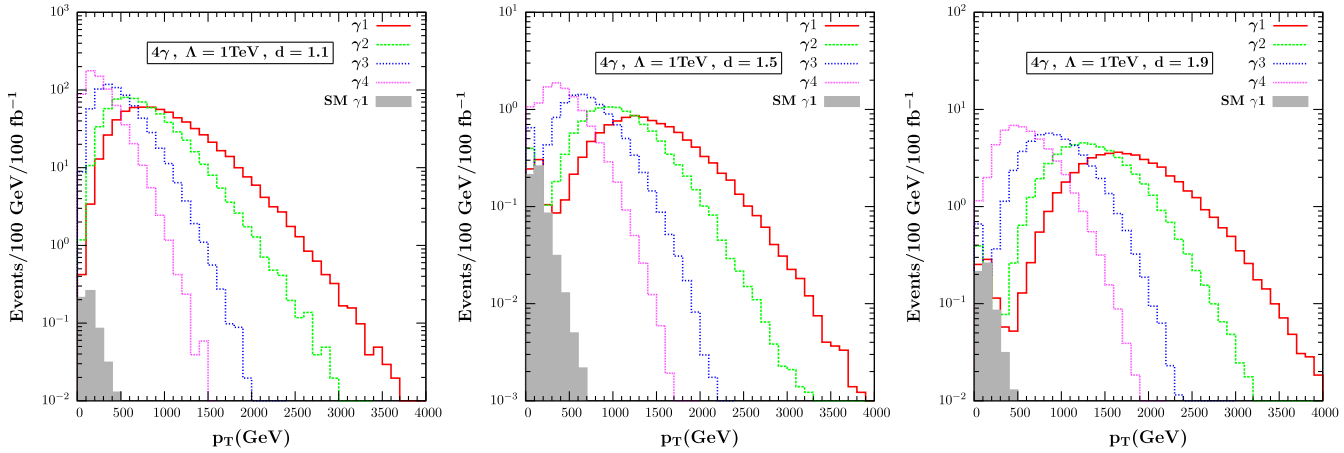

FIG. 4. The p_T distributions of each photon at $\Lambda_{\mathcal{U}} = 1$ TeV for $d = 1.1$, 1.5, and 1.9 within a scalar unparticle scenario. In each case, the largest SM background is depicted.

photon pair production signal can be done with some precision, it gets harder as the number of photons increases and the SM prediction gets suppressed. Therefore, multiphoton signals are testing grounds for different scenarios and the unparticle scenario would be one of them.

In this subsection, we will discuss the four-photon signal within the unparticle framework and then compare it with the SM background. Four-photon event selection requires each photon to have at least 30 GeV transverse momentum (p_T) with a cone separation $\Delta R_{ij} = 0.4$ between any two photons. Pseudorapidity $|\eta_i| \leq 2.44$ is also required for each photon. They are listed in Table II.

The number of events for the signal $pp \to 4\gamma$ at the LHC with the center-of-mass energy 14 TeV and the integrated luminosity 100 fb^{-1} are shown as a function of various variables in Fig. 3. As far as the number of generated jets is concerned, the signal shows almost identical distributions with the largest SM case when $\Lambda_{\mathcal{U}} = 3$ TeV but many more jets can be generated over the background for $\Lambda_{\mathcal{U}} = 1$ TeV. For the case of H_T distributions, the background shows a sharp drop, and H_T gets larger while the signal starts developing a shoulder for all cases with $\Lambda_{\mathcal{U}} = 1$ TeV and for only $d_{\mathcal{U}} = 1.1$ when $\Lambda_{\mathcal{U}}$ is taken 3 TeV. This practically means that heavy particles must be produced so that we get more events with large H_T. Additionally, an optimal H_T cut value could be determined to reduce the background further if needed. The distributions with respect to the cone size for various photon pairs resemble each other (having similar peak patterns) when comparing the signal with the corresponding SM background. The number of background events is just subdued. As far as the topology of the events is concerned, among the hardest three photons, the distance between the hardest photon and the second hardest one peaks at larger values than the distance between the second and the third. Hence, the hardest and the second hardest must come off from different branches. All possible invariant mass distributions are compared with the largest SM background, and an invariant mass cut can further be fixed as well. The number of signal events as a function of the transverse momenta of the photons at a fixed $\Lambda_{\mathcal{U}} = 1$ TeV for various d values are presented in Fig. 4. In each case, only the largest SM background is included, and the photons are labeled in descending order based on their energies. It seems possible to eliminate the background altogether by using an improved cut value. In the case of $d_{\mathcal{U}} = 1.5$ and $d_{\mathcal{U}} = 1.9$, a higher luminosity might be needed for producing enough signal events.

B. $pp \to 2\gamma 2g$ signal

As compared to the 4γ signal, here we require two photons and at least two gluon jets. We expect more events for both the signal and for the background. Our findings are depicted in Figs. 5 and 6. The jet activity for the background is suppressed even at $\Lambda_{\mathcal{U}} = 3$ TeV for $d_{\mathcal{U}} = 1.1$. Also from the H_T distributions, we observe that the signal starts deviating from the background for even low energies at which the signal peaks. ΔR seems to be a useful quantity since the signal and background prefer to have peaks at opposite sites. For the transverse momentum distributions where the hardest photon and the hardest gluon jet distributions are included for the background, the background has almost no tail over 500 GeV, while the signal shows much broader distributions with peaks moving to higher energies as $d_{\mathcal{U}}$ gets larger.

C. $pp \to 2\gamma 2l$ signal

If we consider the signal with two photons and two isolated charged leptons where leptons could be

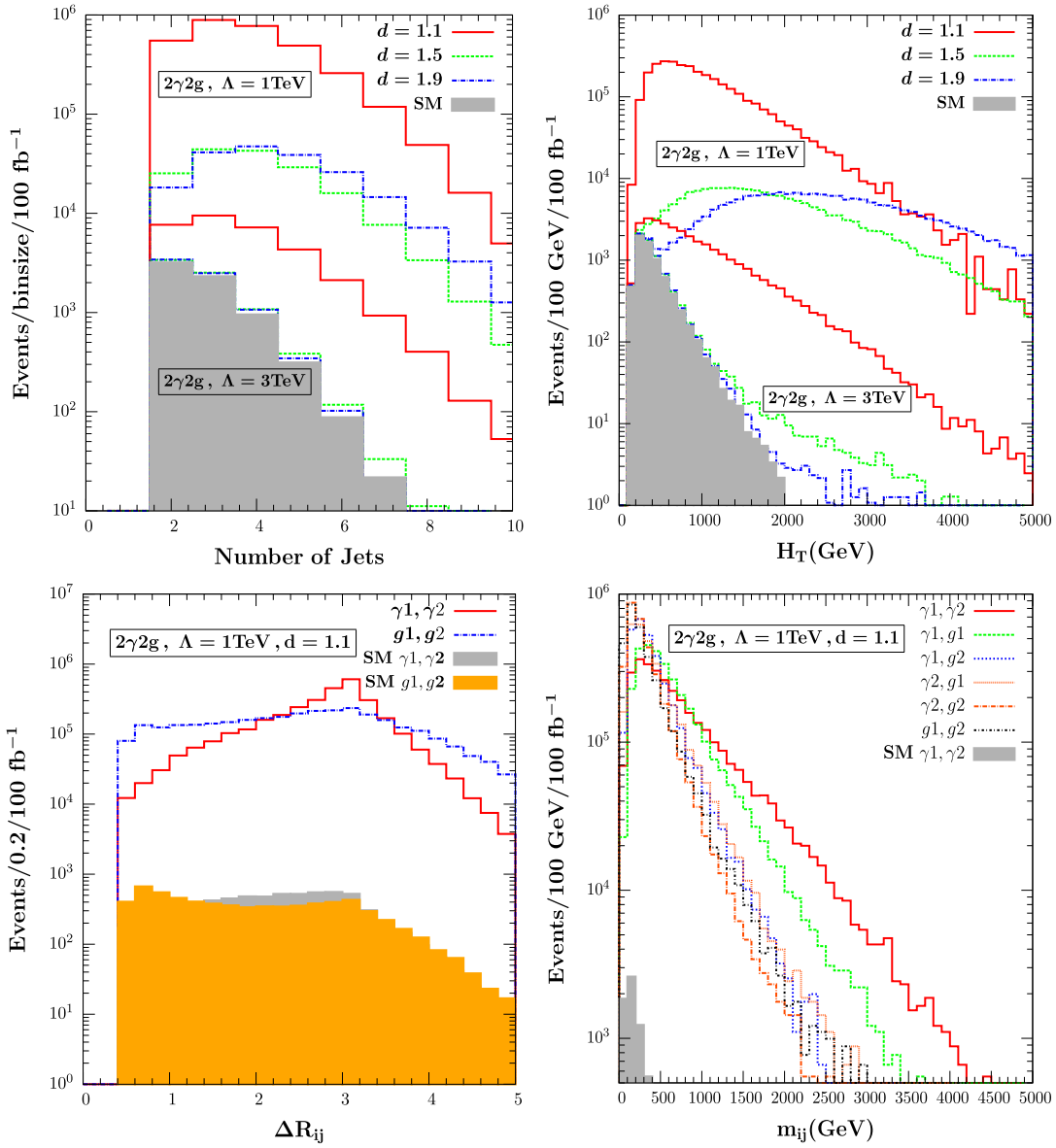

FIG. 5. Various distributions for the $pp \to 2\gamma 2g$ signal within a scalar unparticle scenario for $\Lambda_{\mathcal{U}} = 1$ TeV. In the case of invariant mass distribution, only the largest SM background is shown. For the ΔR_{ij} distributions, two distinct SM backgrounds are preferred to be presented. $\Lambda_{\mathcal{U}} = 3$ TeV case is not included in the ΔR_{ij} and m_{ij} cases since it looks very much like the SM distribution.

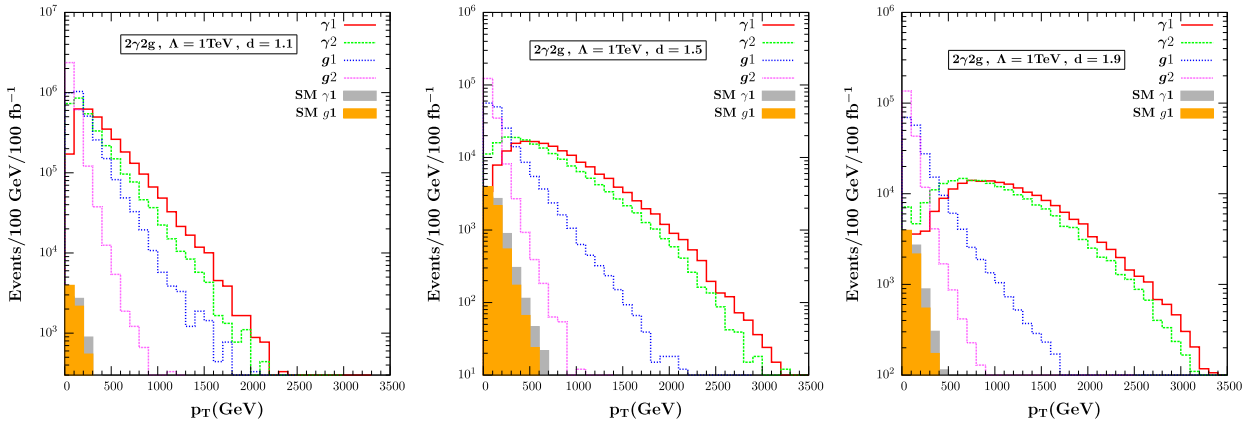

FIG. 6. The p_T distributions of each photon at $\Lambda_{\mathcal{U}} = 1$ TeV for $d_{\mathcal{U}} = 1.1$, 1.5, and 1.9 within a scalar unparticle scenario. In each case, the largest SM background is depicted.

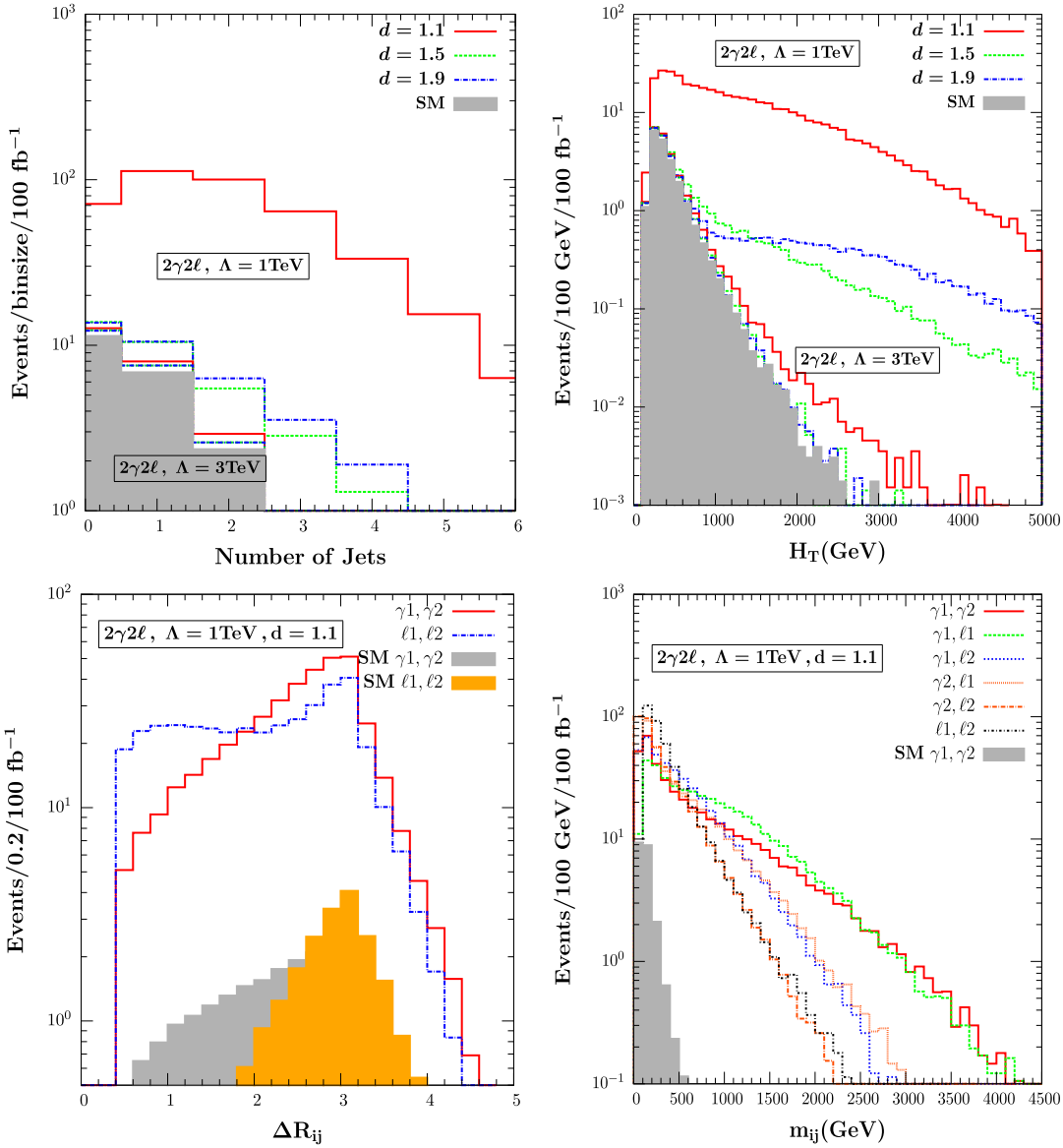

FIG. 7. Various distributions for the $pp \to 2\gamma 2\ell$ signal within a scalar unparticle scenario for $\Lambda_{\mathcal{U}} = 1$ TeV. In the case of invariant mass distribution, only the largest SM background is shown. For the ΔR_{ij} distributions, two distinct SM backgrounds are preferred to be presented. $\Lambda_{\mathcal{U}} = 3$ TeV case is not included in the ΔR_{ij} and m_{ij} cases since it looks very much like the SM distribution.

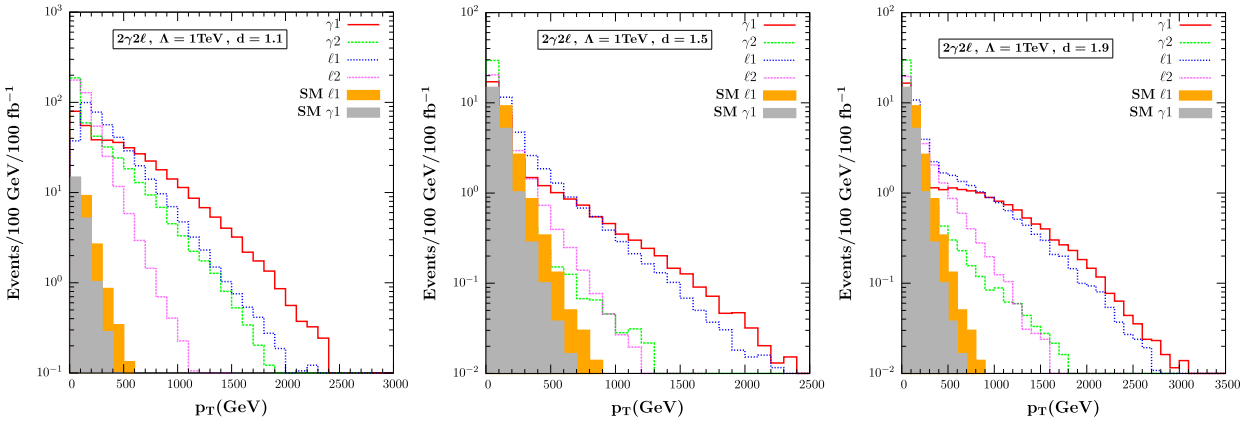

FIG. 8. The p_T distributions of each photon at $\Lambda_{\mathcal{U}} = 1$ TeV for $d_{\mathcal{U}} = 1.1$, 1.5, and 1.9 within a scalar unparticle scenario. In each case, the largest SM background is depicted.

electrons or muons or both, the results are summarized in Figs. 7 and 8. The jet activities for the signal and background resemble each other except for $\Lambda_{\mathcal{U}} = 1$ TeV and $d_{\mathcal{U}} = 1.1$. H_T distribution shows that the signal shrinks to the background for $\Lambda_{\mathcal{U}} = 3$ TeV and above. For $\Lambda_{\mathcal{U}} = 1$ TeV, the signal starts dominating the background around the energy scale 1 TeV. Both the invariant mass and the transverse momenta distributions have similar features, showing enhancement especially at the high-energy tail.

D. $pp \to 2e2\mu$ signal

In this part, we discuss the signal with two isolated electrons and two isolated muons at the LHC. The other possibilities—that is, four electrons or four muons—show very similar features. Even though four-lepton isolation is considered to be a difficult signal to pursue, we nonetheless explore it here as a case study with the results depicted in Figs. 9 and 10. We could conclude that the signal shows some order of magnitude deviations from the background as long as d is small like 1.1 or so. The deviation is there

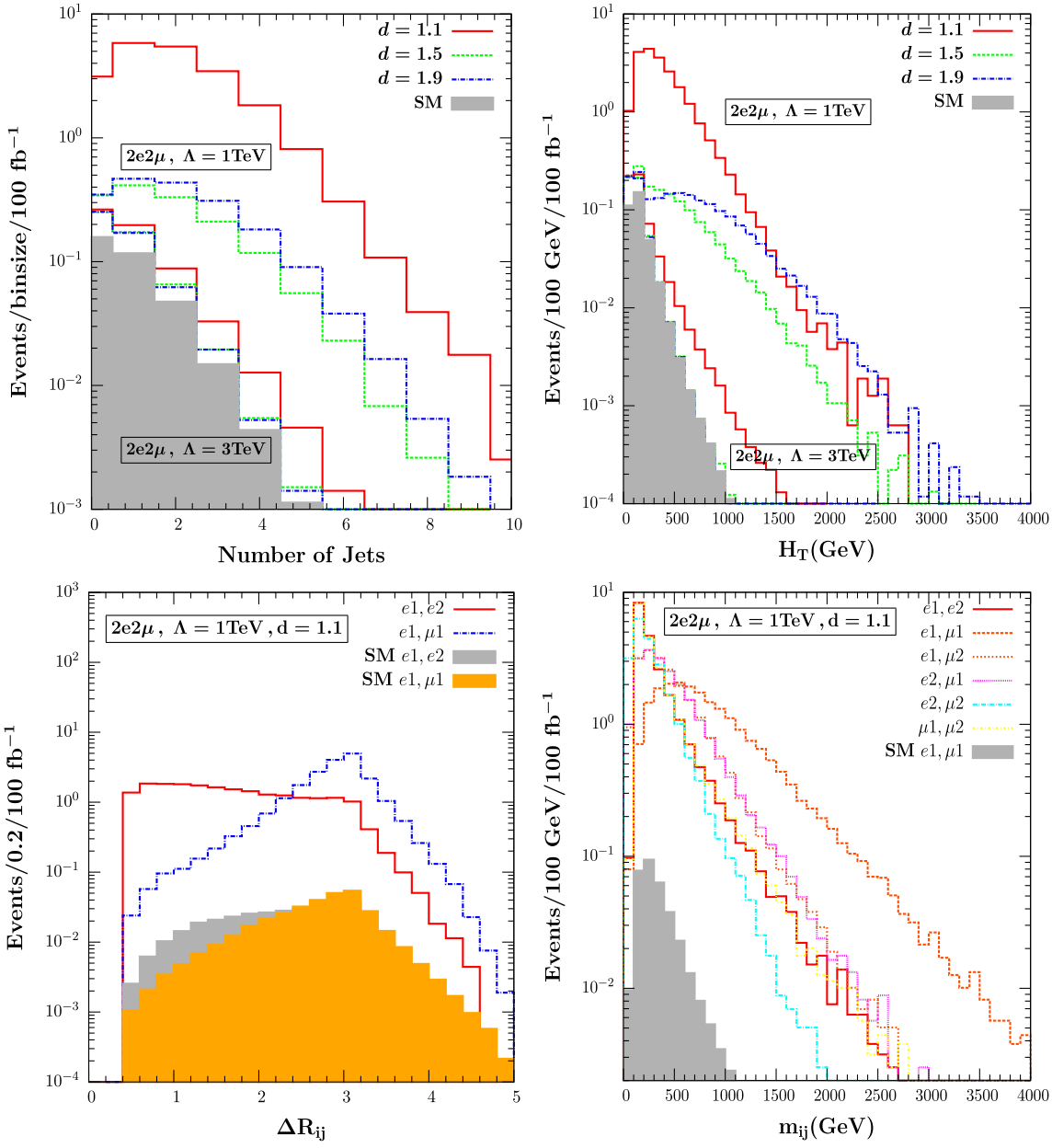

FIG. 9. Various distributions for the $pp \to 2e2\mu$ signal within a scalar unparticle scenario for $\Lambda_{\mathcal{U}} = 1$ TeV. In the case of invariant mass distribution, only the largest SM background is shown. For the ΔR_{ij} distributions, two distinct SM backgrounds are preferred to be presented. $\Lambda_{\mathcal{U}} = 3$ TeV case is not included in the ΔR_{ij} and m_{ij} cases since it looks very much like the SM distribution.

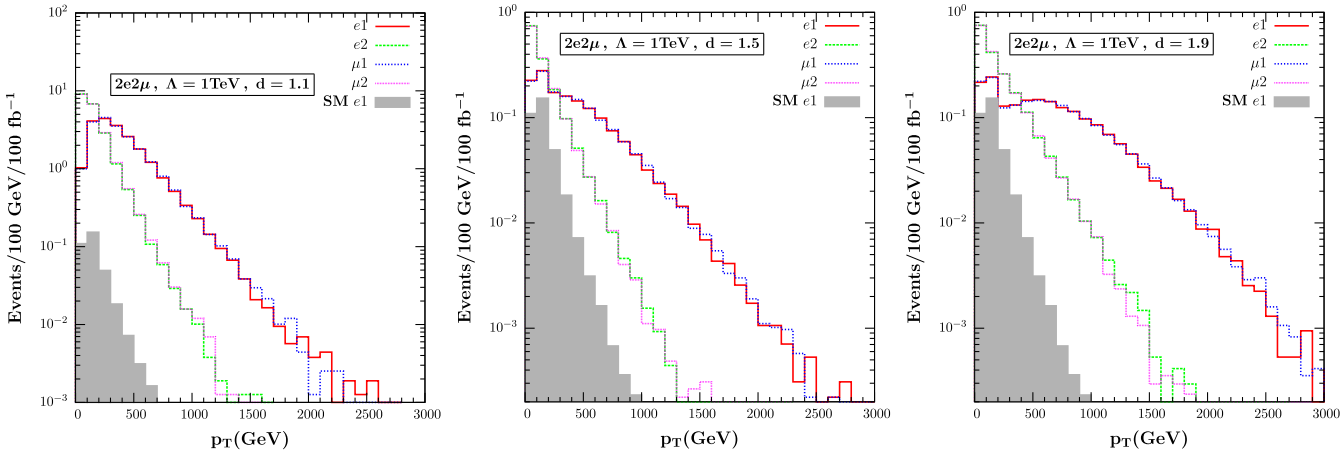

FIG. 10. The p_T distributions of each photon at $\Lambda_{\mathcal{U}} = 1$ TeV for $d = 1.1$, 1.5, and 1.9 within a scalar unparticle scenario. In each case, the largest SM background is depicted.

even for $\Lambda_{\mathcal{U}} = 3$ TeV. However, as we allow d to be larger, only the $\Lambda_{\mathcal{U}} = 1$ TeV case shows profound differences from the background, and as $\Lambda_{\mathcal{U}}$ gets larger, the signal goes below the background where the signal identification would require new techniques.

To summarize the situation and to be able to roughly compare the signals with each other, it would be useful to calculate the significance of each signal, defined as $S/\sqrt{S+B}$ where $S(B)$ is the number of expected signal (background) events. Then any signal with significance

TABLE III. The summary of the numerical analysis of all signals for various $(d_{\mathcal{U}}, \Lambda_{\mathcal{U}})$ values including cross sections, expected signal events as well as the significance defined as $S/\sqrt{S+B}$ where B stands for the background events. The center-of-mass energy is 14 TeV with integrated luminosity 100 fb^{-1}.

Process	$\Lambda_{\mathcal{U}}$	$d_{\mathcal{U}}$	$\sigma(pb)$	S	$\frac{S}{\sqrt{S+B}}$
$pp \to 4\gamma$	1 TeV	1.1	9.792×10^{-3}	949.99 ± 5.32	30.8095 ± 0.0865
		1.5	1.745×10^{-4}	16.890 ± 0.736	4.019 ± 0.098
		1.9	7.665×10^{-4}	74.48 ± 1.45	8.5860 ± 0.0864
	3 TeV	1.1	1.077×10^{-5}	0.95 ± 0.34	0.722 ± 0.199
		1.5	1.018×10^{-5}	0.889 ± 0.336	0.691 ± 0.202
		1.9	1.017×10^{-5}	0.889 ± 0.335	0.691 ± 0.201
$pp \to 2\gamma 2g$	1 TeV	1.1	5.520×10^{1}	1579879 ± 1061	1254.288 ± 0.424
		1.5	3.010×10^{0}	80926 ± 243	273.432 ± 0.453
		1.9	3.798×10^{0}	82830 ± 254	276.872 ± 0.467
	3 TeV	1.1	6.166×10^{-1}	19636 ± 115	121.07 ± 0.47
		1.5	1.826×10^{-1}	7143.3 ± 65.9	60.780 ± 0.439
		1.9	1.797×10^{-1}	7121.5 ± 65.6	60.642 ± 0.437
$pp \to 2\gamma 2l$	1 TeV	1.1	8.117×10^{-3}	737.34 ± 8.22	26.482 ± 0.159
		1.5	7.251×10^{-4}	64.3 ± 2.7	6.360 ± 0.196
		1.9	7.716×10^{-4}	69.50 ± 2.71	6.71 ± 0.19
	3 TeV	1.1	5.060×10^{-4}	44.15 ± 2.37	4.875 ± 0.202
		1.5	4.716×10^{-4}	41.23 ± 2.28	4.6 ± 0.2
		1.9	4.713×10^{-4}	41.13 ± 2.29	4.627 ± 0.201
$pp \to 4l$	1 TeV	1.1	6.310×10^{-4}	55.27 ± 2.62	7.382 ± 0.178
		1.5	4.422×10^{-5}	3.82 ± 0.72	1.778 ± 0.202
		1.9	5.903×10^{-5}	5.222 ± 0.776	2.128 ± 0.184
	3 TeV	1.1	1.304×10^{-5}	1.051 ± 0.452	0.773 ± 0.243
		1.5	1.026×10^{-5}	0.810 ± 0.413	0.639 ± 0.248
		1.9	1.021×10^{-5}	0.806 ± 0.412	0.636 ± 0.248

larger than 5 and having at least 5 signal events could be qualified as a potential venue for tracing new physics effects. Our results are summarized in Table III. The numeric results are generated with the use of MadAnalysis [23].

As seen from the table, the largest significance is for the $pp \to 2\gamma 2g$ case with lots of signal events. It should be noted that the $2\gamma 2g$ signal may not be easy to detect due to gluon jet involvement. For the $pp \to 4\gamma$ case, the unparticle effects are sizable only for $\Lambda_{\mathcal{U}} = 1$ TeV with the scaling parameter d near its boundary values. As compared to the 4γ case, the situation in the $pp \to 2\gamma 2\ell$ case is similar, but even for $\Lambda_{\mathcal{U}} = 3$ TeV, the significance is very close to 5. The background for the $pp \to 4\ell$ is large enough so that the unparticle effects may have a chance to be distinguishable for only $(d_{\mathcal{U}}, \Lambda_{\mathcal{U}}) = (1.1, 1\ \text{TeV})$. It should also be noted that the signal-over-background ratio can be enhanced by doing a further cut optimization, which can be deduced from the distributions shown.

IV. DISCUSSION AND CONCLUSION

If a scale-invariant sector exists and finds ways to interact with the SM fields through heavy mediators, the scenario with some scalar, vector, or tensor unparticle has been realized, and the possibility that the unparticle is indeed a scalar seems to be phenomenologically favored.

In this study, signals with final states—4 photons, 2 photons +2 gluons, 2 photons +2 leptons, and 2 electrons +2 muons in the proton-proton collisions at the LHC at 14 TeV center-of-mass energy—are considered within the framework of the scalar unparticle scenario after implementing the three-point self-interactions of the scalar unparticles in MadGraph while keeping all other possible contributions to the signals.

We first discuss possible bounds on the parameters of the model from the available $pp \to 2\gamma$ analysis with the data at 7 TeV [16]. The signals mentioned above are discussed after putting some basic cuts and compared with the SM predictions. The number of events with integrated luminosity 100 fb^{-1} as a function of various quantities like number of jets, H_T, ΔR_{ij}, m_{ij}, and p_T are depicted. We also summarize the results together with the significance of each signal in Table III. It seems that indirect unparticle effect could be discriminated from the SM predictions in almost all cases if the cutoff scale $\Lambda_{\mathcal{U}}$ is around 1 TeV and for especially small $d_{\mathcal{U}}$ values, close to its lower boundary value and, in some cases, to its upper boundary value as well.

Unparticle effects have been studied also in various different areas, ranging from atomic physics [24–26] to cosmology [27] and colliders [8,17]. On the atomic physics side, the contribution to the ground state energy levels of the hydrogen atom is conducted by taking into account the scalar unparticle potential [24] within the nonrelativistic perturbative approach. It is concluded in [24] that, for $d_{\mathcal{U}} < 1.3$, the bound on $\Lambda_{\mathcal{U}}$ exceeds 1 TeV, which strongly depends on the scalar unparticle couplings to the electron and proton. Those couplings are assumed to be equal to each other.

At the LHC, the unparticle effects have been studied through their real emissions in the monojet and mono-Z channels [17]. The main assumption of these studies is that the unparticles produced through real emission are assumed to live long enough so that they do not decay within the detector. Hence, the large transverse energy imbalance would become the only fingerprint of the unparticle effects. Obviously, the situation is totally different in our case, and such an analysis lies beyond the scope of the current study.

To sum up, we have performed indirect manifestations of unparticles, i.e., as virtual effects, in various channels $(4\gamma, 2\gamma 2\ell, 2\gamma 2g, 4\ell)$. The contributions from the unparticle self-interactions as well as interference between the unparticle diagrams and the SM ones are all taken into account. In addition, the exclusion region in the $(d_{\mathcal{U}},\Lambda_{\mathcal{U}})$ plane is obtained from existing $pp \to 2\gamma$ data. After having enough precision achieved in the ongoing experiments, it is conceivable that efforts at the LHC could make it possible to discriminate the unparticle effects from other scenarios in the future.

ACKNOWLEDGMENTS

We are much obliged to the late beloved Professor Namık Kemal Pak for his constant guidance and endless motivation and for being an ideal colleague. I. T. thanks Turkish Academy of Science (TUBA) for its partial support through TUBA-GEBIP program. I. T. and S. B. thank METU-BAP Grant No. 08-11-2013-028. We thank Olivier Mattelaer for his help in implementing the model in MadGraph.

APPENDIX A: FEYNMAN DIAGRAMS CONTRIBUTING TO THE PROCESSES

In this part, instead of presenting the complete list of the Feynman diagrams contributing to the considered processes, we prefer to give samples of diagrams in Figs. 11–14, corresponding to different topologies in each case.

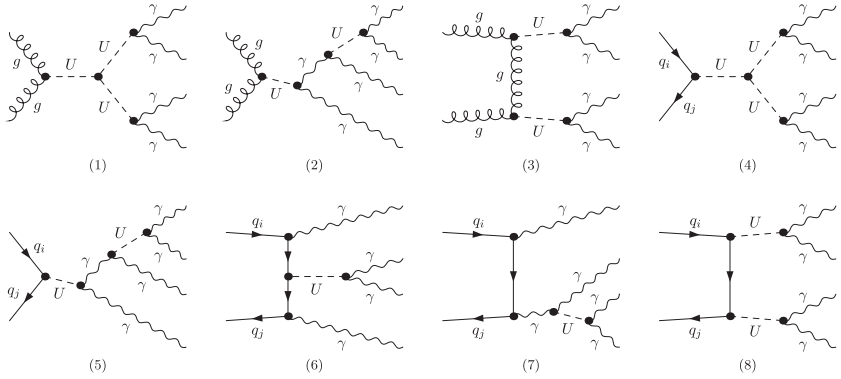

FIG. 11. Selected Feynman diagrams for the process $pp \to 4\gamma$. All possible permutations should be added to get the full list.

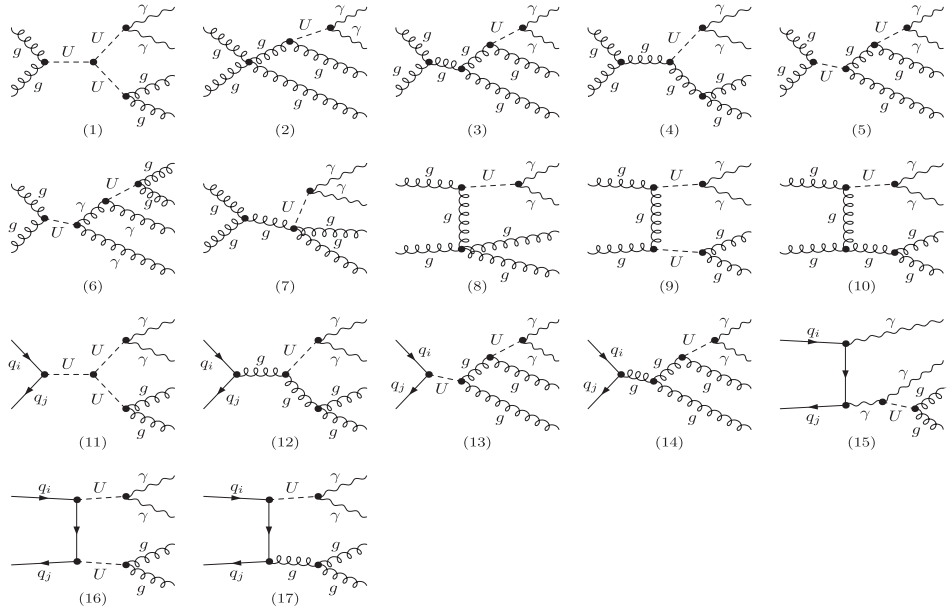

FIG. 12. Selected Feynman diagrams for the process $pp \to 2\gamma 2g$. All possible permutations should be added to get the full list.

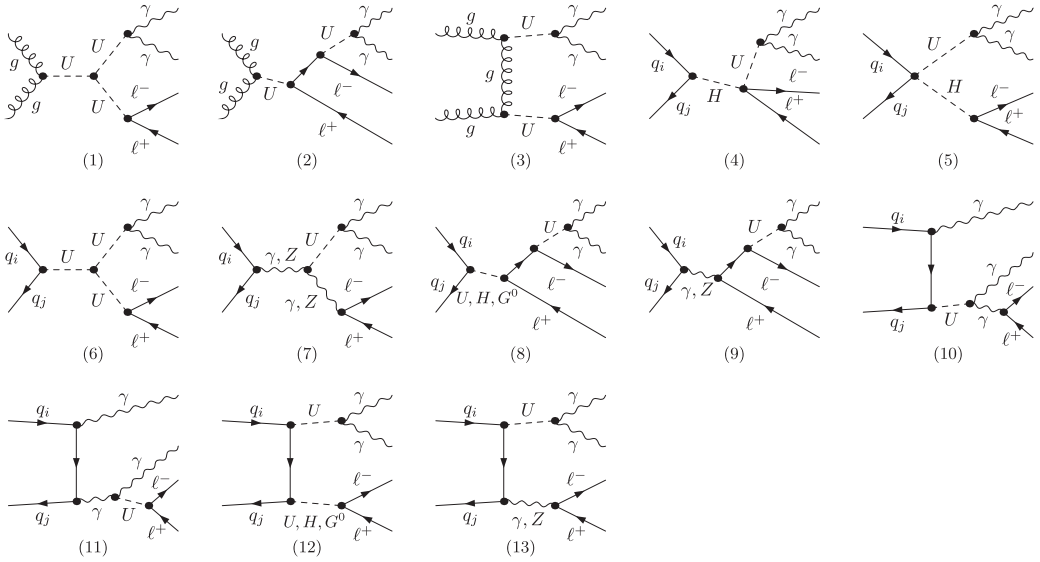

FIG. 13. Selected Feynman diagrams for the process $pp \to 2\gamma \ell^+\ell^-$. Here $\ell = e, \mu$. All possible permutations should be added to get the full list.

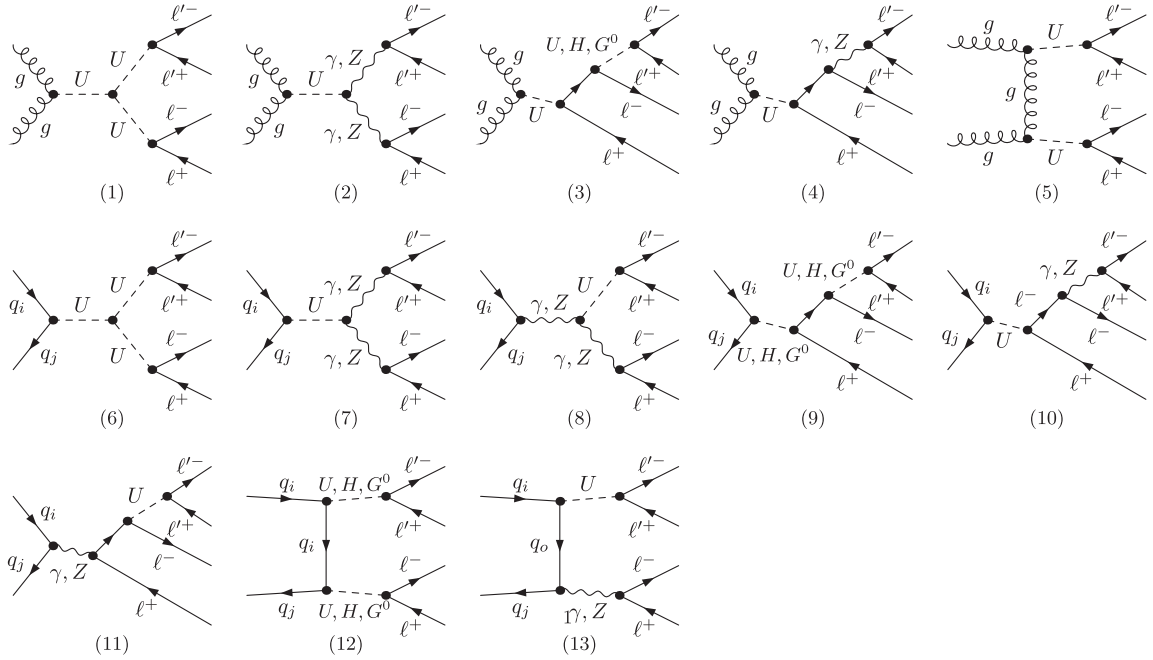

FIG. 14. Selected Feynman diagrams for the process $pp \to \ell^+\ell^-\ell'^+\ell'^-$. Here $\ell, \ell' = e, \mu$. All possible permutations should be added to get the full list.

APPENDIX B: POLYNOMIAL FORMS OF THE THREE-POINT CORRELATION FUNCTION

Here we list, for various $d_{\mathcal{U}}$ values, the fitted form of the F_y function which is written as

$$F_y\left(\frac{p_1^2}{s}, \frac{p_2^2}{s}\right) = 10^{f_y(\log_{10}\frac{p_1^2}{s}, \log_{10}\frac{p_2^2}{s}, d_{\mathcal{U}})}, \tag{B1}$$

where the function $f_y(x, y, d_{\mathcal{U}})$ is assumed to be a sixth-order polynomial with variables x and y.

The explicit form of $f_y(x, y, d_{\mathcal{U}})$ for each $d_{\mathcal{U}}$ value is listed below:

$$\begin{aligned}
f_y(x,y,1.1) = {} & -1.5405271000000 - 0.7774200200000x - 0.7866330300000y + 0.0792432390000x^2 \\
& - 0.0568065580000xy + 0.0536183890000y^2 + 0.0323167350000x^3 - 0.0257729210000x^2y \\
& - 0.0178391900000xy^2 + 0.0113794130000y^3 + 0.0088208374000x^4 - 0.0091290374000x^3y \\
& + 0.0013427708000x^2y^2 - 0.0091546736000xy^3 + 0.0028157322000y^4 + 0.0013727963000x^5 \\
& - 0.0014610970000x^4y - 0.0003212246200x^3y^2 + 0.0008116610800x^2y^3 - 0.0022305525000xy^4 \\
& + 0.0006806753400y^5 + 0.0000870754330x^6 - 0.0000583811290x^5y - 0.0002241075200x^4y^2 \\
& + 0.0004523071200x^3y^3 - 0.0004087510700x^2y^4 + 0.0000568526710xy^5 + 0.0000170296180y^6, \\
f_y(x,y,1.2) = {} & -1.5931413000000 - 0.7289910400000x - 0.7365683400000y + 0.0495076420000x^2 \\
& - 0.0332335900000xy + 0.0276983440000y^2 + 0.0270191700000x^3 - 0.0202016920000x^2y \\
& - 0.0104586380000xy^2 + 0.0084081501000y^3 + 0.0100315200000x^4 - 0.0106389120000x^3y \\
& + 0.0041248972000x^2y^2 - 0.0080704982000xy^3 + 0.0040419030000y^4 + 0.0019167613000x^5 \\
& - 0.0022792017000x^4y + 0.0004435513600x^3y^2 + 0.0005678533700x^2y^3 - 0.0017910916000xy^4 \\
& + 0.0009702022600y^5 + 0.0001383103600x^6 - 0.0001455056900x^5y - 0.0001537687100x^4y^2 \\
& + 0.0004309380400x^3y^3 - 0.0004127246000x^2y^4 + 0.0000962308500xy^5 + 0.0000340802980y^6,
\end{aligned}$$

$$f_y(x,y,1.3) = -1.6410233000000 - 0.6831394500000x - 0.6839238600000y + 0.0098356018000x^2 - 0.0061022750000xy + 0.0094178007000y^2 + 0.0060856850000x^3 - 0.0046300120000x^2y - 0.0048812233000xy^2 + 0.0092921323000y^3 + 0.0028227822000x^4 - 0.0043816065000x^3y + 0.0042084365000x^2y^2 - 0.0063283361000xy^3 + 0.0059037593000y^4 + 0.0006131535500x^5 - 0.0010425094000x^4y + 0.0005225122400x^3y^2 + 0.0003664327100x^2y^3 - 0.0013713355000xy^4 + 0.0013363554000y^5 + 0.0000470772780x^6 - 0.0000616165740x^5y - 0.0000958230540x^4y^2 + 0.0003070295000x^3y^3 - 0.0003082150200x^2y^4 + 0.0000764330580xy^5 + 0.0000649171240y^6,$$

$$f_y(x,y,1.4) = -1.6842770000000 - 0.6268423200000x - 0.6338316600000y + 0.0055970389000x^2 + 0.0139964740000xy - 0.0145320950000y^2 + 0.0192604490000x^3 - 0.0026778417000x^2y + 0.0034019656000xy^2 - 0.0004070407400y^3 + 0.0102869040000x^4 - 0.0068507861000x^3y + 0.0059080722000x^2y^2 - 0.0031578032000xy^3 + 0.0017214913000y^4 + 0.0021861777000x^5 - 0.0020625485000x^4y + 0.0013463745000x^3y^2 - 0.0001467668100x^2y^3 - 0.0003119999900xy^4 + 0.0002904937700y^5 + 0.0001643119500x^6 - 0.0001700669500x^5y + 0.0000040501655x^4y^2 + 0.0002493650600x^3y^3 - 0.0003028055500x^2y^4 + 0.0001574897700xy^5 - 0.0000238051790y^6,$$

$$f_y(x,y,1.5) = -1.7239823000000 - 0.5841207000000x - 0.5835451200000y - 0.0329579040000x^2 + 0.0277305850000xy - 0.0249275450000y^2 - 0.0061406726000x^3 + 0.0071845036000x^2y + 0.0009698820400xy^2 + 0.0067371962000y^3 - 0.0005908533400x^4 + 0.0009089441600x^3y + 0.0018573577000x^2y^2 - 0.0039214458000xy^3 + 0.0065187567000y^4 - 0.0000746652690x^5 + 0.0003873853700x^4y - 0.0003799170600x^3y^2 + 0.0003096119100x^2y^3 - 0.0008651676500xy^4 + 0.0014011978000y^5 - 0.0000091955711x^6 + 0.0000704813420x^5y - 0.0001640648600x^4y^2 + 0.0002406092800x^3y^3 - 0.0002385580800x^2y^4 + 0.0000744175370xy^5 + 0.0000706166990y^6,$$

$$f_y(x,y,d_1.6) = -1.7574221000000 - 0.5296548400000x - 0.5320717200000y - 0.0381500120000x^2 + 0.0478045870000xy - 0.0410908730000y^2 + 0.0011269690000x^3 + 0.0108900100000x^2y + 0.0084243263000xy^2 + 0.0004794936600y^3 + 0.0036834885000x^4 - 0.0011481639000x^3y + 0.0049334989000x^2y^2 - 0.0018404656000xy^3 + 0.0035994200000y^4 + 0.0008605367100x^5 - 0.0006515736200x^4y + 0.0008031427900x^3y^2) - 0.0000690085460x^2y^3 - 0.0001479700300xy^4 + 0.0006790255900y^5 + 0.0000633053100x^6 - 0.0000456439360x^5y - 0.0000330677610x^4y^2 + 0.0001861850800x^3y^3 - 0.0002131552700x^2y^4 + 0.0001142648200xy^5 + 0.0000146061000y^6,$$

$$f_y(x,y,d_1.7) = -1.7859310000000 - 0.4819532800000x - 0.4808190400000y - 0.0568205160000x^2 + 0.0601820280000xy - 0.0510483810000y^2 - 0.0085626578000x^3 + 0.0157293060000x^2y + 0.0118361580000xy^2 - 0.0015692444000y^3 - 0.0003973136300x^4 + 0.0020748123000x^3y + 0.0033761192000x^2y^2 + 0.0002446355700xy^3 + 0.0026363003000y^4 + 0.0000200407320x^5 + 0.0002556639700x^4y + 0.0002493241300x^3y^2 + 0.0001335396100x^2y^3 + 0.0000923550460xy^4 + 0.0004898155200y^5 - 0.0000000764952x^6 + 0.0000324266770x^5y - 0.0000549079190x^4y^2 + 0.0001259923600x^3y^3 - 0.0001257337300x^2y^4 + 0.0000846048940xy^5 + 0.0000097441803y^6,$$

$$
\begin{aligned}
f_y(x,y,1.8) = {} & -1.8082217000000 - 0.4311959700000x - 0.4321981400000y - 0.0614003580000x^2 \\
& + 0.0681025750000xy - 0.0630279150000y^2 - 0.0052333005000x^3 + 0.0147989660000x^2y \\
& + 0.0142681270000xy^2 - 0.0062819835000y^3 + 0.0015725778000x^4 + 0.0005401446100x^3y \\
& + 0.0041388541000x^2y^2 + 0.0004103011300xy^3 + 0.0010780395000y^4 + 0.0004473018100x^5 \\
& - 0.0001973343900x^4y + 0.0004299858200x^3y^2 + 0.0002349362300x^2y^3 - 0.0000267569530xy^4 \\
& + 0.0002615601200y^5 + 0.0000327805430x^6 - 0.0000127250450x^5y - 0.0000178441340x^4y^2 \\
& + 0.0000848834490x^3y^3 - 0.0000701021930x^2y^4 + 0.0000425878570xy^5 + 0.0000031287267y^6, \\
f_y(x,y,1.9) = {} & -1.8230678000000 - 0.3813089500000x - 0.3805333500000y - 0.0644029630000x^2 \\
& + 0.0692731770000xy - 0.0617737870000y^2 - 0.0037091815000x^3 + 0.0127173990000x^2y \\
& + 0.0135749080000xy^2 - 0.0010125714000y^3 + 0.0023442925000x^4 - 0.0000228801960x^3y \\
& + 0.0028946364000x^2y^2 + 0.0005196745700xy^3 + 0.0034504318000y^4 + 0.0005942434900x^5 \\
& - 0.0002497974400x^4y + 0.0001526318300x^3y^2 + 0.0002040476400x^2y^3 - 0.0000738331010xy^4 \\
& + 0.0007605124000y^5 + 0.0000429606120x^6 - 0.0000158586280x^5y - 0.0000256402560x^4y^2 \\
& + 0.0000515125370x^3y^3 - 0.0000392382300x^2y^4 + 0.0000179126770xy^5 + 0.0000458076720y^6.
\end{aligned}
\tag{B2}
$$

[1] G. Aad *et al.* (ATLAS), Observation of a new particle in the search for the Standard Model Higgs boson with the ATLAS detector at the LHC, Phys. Lett. B **716**, 1 (2012).

[2] S. Chatrchyan *et al.* (CMS), Observation of a new boson at a mass of 125 GeV with the CMS experiment at the LHC, Phys. Lett. B **716**, 30 (2012).

[3] H. Georgi, Unparticle Physics, Phys. Rev. Lett. **98**, 221601 (2007).

[4] H. Georgi, Another odd thing about unparticle physics, Phys. Lett. B **650**, 275 (2007).

[5] J. L. Feng, A. Rajaraman, and H. Tu, Unparticle self-interactions and their collider implications, Phys. Rev. D **77**, 075007 (2008).

[6] H. Georgi and Y. Kats, Unparticle self-interactions, J. High Energy Phys. 02 (2010) 065.

[7] J. Bergstrom and T. Ohlsson, Unparticle self-interactions at the Large Hadron Collider, Phys. Rev. D **80**, 115014 (2009).

[8] K. Cheung, W.-Y. Keung, and T.-Chiang Yuan, Collider Signals of Unparticle Physics, Phys. Rev. Lett. **99**, 051803 (2007); Collider Phenomenology of Unparticle Physics, Phys. Rev. D **76**, 055003 (2007); Unparticle phenomenology: A mini review, in *Proceedings, 16th International Conference on Supersymmetry and the Unification of Fundamental Interactions (SUSY08): Seoul, Korea, 2008*, *AIP Conf. Proc.* 1078, 156 (2009).

[9] T. M. Aliev, M. Frank, and I. Turan, Collider effects of unparticle interactions in multiphoton signals, Phys. Rev. D **80**, 114019 (2009).

[10] B. Grinstein, K. A. Intriligator, and I. Z. Rothstein, Comments on unparticles, Phys. Lett. B **662**, 367 (2008).

[11] J. Alwall, M. Herquet, F. Maltoni, O. Mattelaer, and T. Stelzer, MadGraph 5: Going beyond, J. High Energy Phys. 06 (2011) 128.

[12] A. Delgado and M. J. Strassler, A Simple-minded unitarity constraint and an application to unparticles, Phys. Rev. D **81**, 056003 (2010); F. Caracciolo and V. S. Rychkov, Rigorous limits on the interaction strength in quantum field theory, Phys. Rev. D **81**, 085037 (2010).

[13] C. Degrande, C. Duhr, B. Fuks, D. Grellscheid, O. Mattelaer, and T. Reiter, UFO—The Universal Feynrules output, Comput. Phys. Commun. **183**, 1201 (2012).

[14] A. Alloul, N. D. Christensen, C. Degrande, C. Duhr, and B. Fuks, FeynRules 2.0—A complete toolbox for tree-level phenomenology, Comput. Phys. Commun. **185**, 2250 (2014).

[15] P. de Aquino, W. Link, F. Maltoni, O. Mattelaer, and T. Stelzer, ALOHA: Automatic Libraries Of Helicity Amplitudes for Feynman Diagram Computations, Comput. Phys. Commun. **183**, 2254 (2012).

[16] S. Chatrchyan *et al.* (CMS), Measurement of the production cross section for pairs of isolated photons in pp collisions at $\sqrt{s} = 7$ TeV, J. High Energy Phys. 01 (2012) 133.

[17] S. Chatrchyan *et al.* (CMS Collaboration), Search for New Physics with a Monojet and Missing Transverse Energy in pp Collisions at $\sqrt{s} = 7$ TeV, Phys. Rev. Lett. **107**, 201804 (2011); V. Khachatryan *et al.* (CMS), Search for dark matter, extra dimensions, and unparticles in monojet events in proton-proton collisions at $\sqrt{s} = 8$ TeV, Eur. Phys. J. C **75**, 235 (2015); A. M. Sirunyan *et al.* (CMS), Search for dark matter and unparticles in events with a Z boson and missing transverse momentum in proton-proton collisions at $\sqrt{s} = 13$ TeV, J. High Energy Phys. 03 (2017) 061.

[18] J. Alwall, R. Frederix, S. Frixione, V. Hirschi, F. Maltoni, O. Mattelaer, H. S. Shao, T. Stelzer, P. Torrielli, and M. Zaro, The automated computation of tree-level and next-to-leading order differential cross sections, and their matching to parton shower simulations, J. High Energy Phys. 07 (2014) 079.

[19] T. Sjostrand, S. Mrenna, and P. Z. Skands, PYTHIA 6.4 physics and manual, J. High Energy Phys. 05 (2006) 026; T. Sjöstrand, S. Ask, J. R. Christiansen, R. Corke, N. Desai, P. Ilten, S. Mrenna, S. Prestel, C. O. Rasmussen, and P. Z. Skands, An Introduction to PYTHIA 8.2, Comput. Phys. Commun. **191**, 159 (2015).

[20] G. Aad *et al.* (ATLAS), Search for resonances decaying into top-quark pairs using fully hadronic decays in pp collisions with ATLAS at $\sqrt{s} = 7$ TeV, J. High Energy Phys. 01 (2013) 116.

[21] H. L. Lai, J. Huston, S. Kuhlmann, F. I. Olness, J. F. Owens, D. E. Soper, W. K. Tung, and H. Weerts, Improved parton distributions from global analysis of recent deep inelastic scattering and inclusive jet data, Phys. Rev. D **55**, 1280 (1997); A. D. Martin, R. G. Roberts, W. James Stirling, and R. S. Thorne, Parton distributions and the LHC: W and Z production, Eur. Phys. J. **C14**, 133 (2000); M. Werlen *et al.*, A new determination of α_s using direct photon production cross sections in pp and $\bar{p}p$ collisions at $\sqrt{s}$= 24.3 GeV, Phys. Lett. B **452**, 201 (1999).

[22] T. Orimoto (CMS), Search for new physics in the low MET monophoton channel with the CMS Detector, in *Proceedings, Meeting of the APS Division of Particles and Fields (DPF 2015): Ann Arbor, Michigan, USA, 2015,* arXiv:1511.00337; G. Aad *et al.* (ATLAS), Search for new phenomena in events with at least three photons collected in pp collisions at $\sqrt{s} = 8$ TeV with the ATLAS detector, Eur. Phys. J. C **76**, 210 (2016).

[23] B. Dumont, B. Fuks, S. Kraml, S. Bein, G. Chalons, E. Conte, S. Kulkarni, D. Sengupta, and C. Wymant, Toward a public analysis database for LHC new physics searches using MADANALYSIS 5, Eur. Phys. J. C **75**, 56 (2015); E. Conte, B. Dumont, B. Fuks, and C. Wymant, Designing and recasting LHC analyses with MadAnalysis 5, Eur. Phys. J. C **74**, 3103 (2014); E. Conte, B. Fuks, and G. Serret, MADANALYSIS 5, A user-friendly framework for collider phenomenology, Comput. Phys. Commun. **184**, 222 (2013).

[24] M. F. Wondrak, P. Nicolini, and M. Bleicher, Unparticle contribution to the hydrogen atom ground state energy, Phys. Lett. B **759**, 589 (2016).

[25] J. P. F. LeBlanc and A. G. Grushin, Unparticle mediated superconductivity, New J. Phys. **17**, 033039 (2015).

[26] A. M. Frassino, P. Nicolini, and O. Panella, Un-Casimir effect, arXiv:1311.7173.

[27] S. Hannestad, G. Raffelt, and Y. Y. Y. Wong, Unparticle constraints from SN 1987A, Phys. Rev. D **76**, 121701 (2007); P. K. Das, Unparticle effects in Supernovae cooling, Phys. Rev. D **76**, 123012 (2007); A. Freitas and D. Wyler, Astro unparticle physics, J. High Energy Phys. 12 (2007) 033; H. Davoudiasl, Constraining Unparticle Physics with Cosmology and Astrophysics, Phys. Rev. Lett. **99**, 141301 (2007); J. McDonald, Cosmological constraints on unparticles, J. Cosmol. Astropart. Phys. 03 (2009) 019.